



Relevance of processing parameters for grain growth of metal halide perovskites with nanoimprint

Andre Mayer¹ · Tobias Haeger² · Manuel Runkel² · Johannes Rond¹ · Johannes Staabs¹ · Frederic van gen Hassend³ · Arne Röttger³ · Patrick Görrn^{1,5} · Thomas Riedl^{2,5} · Hella-Christin Scheer⁴

Received: 20 July 2021 / Accepted: 1 August 2021 / Published online: 28 August 2021
© The Author(s) 2021

Abstract

The quality and the stability of devices prepared from polycrystalline layers of organic–inorganic perovskites highly depend on the grain sizes prevailing. Tuning of the grain size is either done during layer preparation or in a post-processing step. Our investigation refers to thermal imprint as the post-processing step to induce grain growth in perovskite layers, offering the additional benefit of providing a flat surface for multi-layer devices. The material studied is MAPbBr₃; we investigate grain growth at a pressure of 100 bar and temperatures of up to 150 °C, a temperature range where the pressurized stamp is beneficial to avoid thermal degradation. Grain coarsening develops in a self-similar way, featuring a log-normal grain size distribution; categories like ‘normal’ or ‘secondary’ growth are less applicable as the layers feature a preferential orientation already before imprint-induced grain growth. The experiments are simulated with a capillary-based growth law; the respective parameters are determined experimentally, with an activation energy of $Q \approx 0.3$ eV. It turns out that with imprint as well the main parameter relevant to grain growth is temperature; to induce grain growth in MAPbBr₃ within a reasonable processing time a temperature of 120 °C and beyond is advised. An analysis of the mechanical situation during imprint indicates a dominance of thermal stress. The minimization of elastic energy and surface energy together favours the development of grains with (100)-orientation in MAPbBr₃ layers. Furthermore, the experiments indicate that the purity of the materials used for layer preparation is a major factor to achieve large grains; however, a diligent and always similar preparation of the layer is equally important as it defines the pureness of the resulting perovskite layer, intimately connected with its capability to grow. The results are not only of interest to assess the potential of a layer with respect to grain growth when specific temperatures and times are chosen; they also help to rate the long-term stability of a layer under temperature loading, e.g. during the operation of a device.

Keywords Thermal imprint · Methylammonium lead bromide perovskite · Grain growth · Grain size distribution · Growth law · Activation energy · Thermal stress · Simulation

✉ Andre Mayer
amayer@uni-wuppertal.de

¹ Chair of Large Area Optoelectronics, School of Electrical, Information and Media Engineering, University of Wuppertal, Rainer-Gruenter-Str. 21, 42119 Wuppertal, Germany

² Chair of Electronic Devices, School of Electrical, Information and Media Engineering, University of Wuppertal, Rainer-Gruenter-Str. 21, 42119 Wuppertal, Germany

³ Chair for Novel Manufacturing Technologies and Materials, University of Wuppertal, Bahnhofstr. 15, 42651 Solingen, Germany

⁴ School of Electrical, Information and Media Engineering, University of Wuppertal, Rainer-Gruenter-Str. 21, 42119 Wuppertal, Germany

⁵ Wuppertal Center for Smart Materials & Systems, Rainer-Gruenter-Str. 21, 42119 Wuppertal, Germany

1 Introduction

Thin film devices typically have to rely on the properties of their layers [1] being either amorphous or polycrystalline. With polycrystalline layers, the size of the crystallites depends on the preparation method and the procedure followed. The morphology of the layers determines all, their mechanical [2, 3], their thermal [4, 5] and their electrical properties [6, 7]. With semiconductors, generation/recombination represents a further issue, determining e.g. the optical properties [2, 8]. As the defects associated with grain boundaries may induce losses, their volumetric fraction should be low compared to that of the ordered grains. As a consequence, the grain size is a crucial parameter, not only with conventional semiconductors like Si [9–11], but also with a number of currently emerging materials, such as halide perovskites [12–15].

The grain size can be regulated either during or after layer deposition [16]. In view of large grains, the latter is of benefit [17, 18]; post-processing alleviates the demands on the formation of the layer itself and postpones the achievement of large grains to a subsequent step, thus facilitating the control of the overall process. Most often the post-processing step is a simple thermal annealing [15, 17, 19], e.g. under inert atmosphere. Our investigation concentrates on thermal imprint as the post-processing step [20–24] to induce grain growth with polycrystalline layers of metal halide perovskites.

Grain growth during thermal annealing was investigated with metals [17, 19, 25] and conventional semiconductors [19, 26–28]; it involves the movement of grain boundaries, a diffusion-related process promoted by temperature. In particular, the grain growth in polycrystalline layers is known to feature specific characteristics. As long as the grains are small (small compared to the layer thickness), they grow in three dimensions, as in a bulk material. Basically, growth is capillary driven; the mean curvature of the grain surface decreases with ongoing grain growth. However, this ‘normal’ growth comes to a stagnation when the grains span the thickness of the layer, forming a columnar structure. A stagnation of growth (the so-called specimen thickness effect [1, 28–30]) is due to the role of the surfaces of the layer. Whereas in 3D-growth the overall energy of the system is characterized by the curvature and just the energy of the interfaces between the grains (the grain boundary energy, γ_{gb}), 2D-growth in layers with columnar grains additionally involves the energy of the free surface, γ_{s0} , and the energy of the interface to the substrate, γ_{sub} , the more the larger the respective lateral areas of the grains. As a consequence, it was found that the grain size of a thin layer features an upper limit in the range of 2–3 times the layer thickness h [1, 17, 28].

As to be expected from its physical roots, the mean grain radius then is dictated by these additional parameters compared to γ_{gb} and amounts to about $h \cdot \gamma_{s0}/\gamma_{gb}$; this relation assumes a force balance of γ_{gb} and γ_{s0} at the surface [29] but neglects anisotropy effects [30, 31]. With normal grain growth at stagnation, the grain size follows a log-normal distribution; the orientation of the grains with respect to the substrate is random.

Grain growth beyond stagnation (‘abnormal’ or ‘secondary’ growth) is caused by anisotropy effects [1, 17, 26]. Whereas grain boundary energies are largely independent from orientation, surface/interface energies of a crystal are not [32]; γ_{s0} depends on orientation. With secondary growth, grains with a low surface (and interface) energy grow further by absorbing the grains with a higher surface energy, until all grains are secondary grains. During this secondary growth, a bimodal grain size distribution exists, with an increasing mean size of these secondary grains that overlaps (and more and more dominates) the former stagnated distribution; the final secondary grains again exhibit a single log-normal distribution. Typically, secondary grains feature a preferential orientation in vertical direction, a ‘texture’ [17], exposing their lowest energy surface; the lateral orientation of the single grains is random, with distinct grain boundaries in between. A non-random lateral orientation would require, in addition, a crystalline substrate as present, for example, with Si. Such an ‘epitaxial’ growth [16, 25] tolerates just a selected number of lateral orientations, with small-angle grain boundaries between the final secondary grains.

One of the questions to be answered by the present investigation is to what extent these concepts can be transferred/applied, on the one hand, to polycrystalline layers of organic–inorganic metal halide perovskites and, on the other hand, to thermal imprint as the post-processing technique. It has already been shown that thermal imprint in fact induces grain growth in perovskite layers [13, 20, 21, 33]. Earlier work [21] has even demonstrated that thermal imprint is comparable to annealing under nitrogen as the layer is tightly confined between stamp and substrate during imprint due to the pressure applied; the stamp acts as a cover that shields the layer from the environment, thus enabling processing under ambient air at elevated temperature without layer degradation. Furthermore, after imprint the perovskite surface reproduces the flat or structured surface of the stamp.

The current investigation focusses on grain growth in polycrystalline layers of methylammonium lead bromide (MAPbBr₃) by means of thermal imprint. To induce grain growth, the heated layer is pressed by a flat stamp (‘planar hot pressing’, PHP). In order to identify the dominating driver for grain growth during PHP, we perform experiments under ‘hot loading’ conditions, i.e. introducing the sample in the pre-heated imprint system; by thus skipping the equipment-specific heat-up phase, experiments at well-defined

imprint conditions (temperature T_{imp} , pressure p_{imp} , time t_{imp}) are feasible in order to identify the impact of temperature and pressure on grain growth. To enable swift loading, the imprint stack (sample and stamp) is wrapped together in an Al foil. As the stamp is smaller than the perovskite-covered substrate, every imprinted sample features both, a region covered by the stamp under imprint pressure and a region without stamp that was simply annealed. This allows evaluating the grain size after imprint with and without pressurized stamp under otherwise identical conditions. To follow the progression of grain growth, the imprint time is varied. Complementary experiments with thermal annealing under nitrogen provide information on grain growth without imprint, i.e. during conventional post-treatment, for the purpose of direct comparison.

A number of factors may affect grain growth during thermal imprint. The most obvious are the external control parameters pressure and temperature, and our primary goal is to understand their influence. However, additional imprint-specific parameters may be involved that largely preclude external control. For instance, the preparation of continuous layers requires a high-energy substrate to improve the wetting with the perovskite solution; conversely, the separation of the stamp from the sample after imprint requires a low surface energy of the stamp. For a successful imprint, these parameters should not be varied substantially; we leave them unchanged. Furthermore, the coefficient of thermal expansion of the perovskite differs from that of the substrate (and stamp) so that thermal stresses are inevitable when temperature changes; thermal stress is also known to affect grain growth, e.g. with metals [17, 29]. We will address these factors in context with the experimental findings.

Finally, with the impact of temperature and pressure at hand, we will complement the experimental findings with simulations using a capillary-based growth law [19]; the parameters required therefore are extracted from the experiments. These simulations are appropriate to mirror the grain growth observed; moreover, they reveal the prospects and the limitations of post-processing by thermal imprint in order to induce grain growth in perovskite layers, by the choice of the processing parameters and of the material.

The present reasoning is not only appropriate for imprint with a flat stamp but also for imprint with a patterned stamp. It is the basis for a direct patterning of perovskite layers in view of thin film devices and, moreover, for assessing their thermal integrity under operation.

2 Experimental

The experiments were performed with spin-coated perovskite layers on silicon substrates. The precursor solution contains 504 mg methylammonium bromide, MABr (purity

99.999%, Dyesol) and 488 mg lead acetate, $Pb(AcO)_2$ (purity 98%, TCI). For comparison, also a lead acetate trihydrate was used (purity 99.999%, Sigma-Aldrich) applying an adapted recipe as investigated in detail earlier [21]. The components were mixed together in 1 ml anhydrous dimethylformamide, DMF (purity 99.99%, Sigma Aldrich), and the solution was stirred for 24 h at 60 °C. Then, the layers were prepared by spin coating and soft baking; the respective parameters are 5000 rpm, 3 min and 75 °C or 125 °C, 2 min. The whole layer preparation took place in nitrogen atmosphere; the procedure is similar to Ref. [23]. Directly before spin coating, the substrates were cleaned with citric acid (wiping with a cotton bud) followed by a 15-min treatment with deionized water and isopropanol in an ultrasonic bath. Finally, the surface was activated by VUV treatment with an excimer lamp for 1 min (XERADEX 20, Radium, Germany), resulting in a surface energy of the substrate of 60–70 mN/m [34] to improve wetting. Even with this pre-treatment of the substrate, the layer morphology varied somewhat from sample to sample, with more notable variations from batch to batch.

For the imprint experiments, a proprietary system was used (for characteristics see [35, 36]). This system offers high experimental flexibility; it enables e.g. short-time imprints and loading at processing temperature as required for the current investigation. Our standard process for the imprint of perovskites is shown in Fig. 1a; when a flat stamp (here a piece of silicon) is used, we call this ‘planar hot pressing’, PHP. When the imprint stack is loaded, the pressure is applied first; this assures a tight contact between stamp and sample and seals the perovskite from the ambient atmosphere, thus preventing the layer from degradation [21]. Then, the temperature is raised and held constant for the imprint time, followed by a cool down to room temperature where the imprint stack is unloaded [23]. With $MAPbBr_3$, common imprint parameters are a pressure of $p_{imp} = 100$ bar, a temperature of $T_{imp} = 150$ °C and a time of $t_{imp} = 5$ min.

To get the idea of grain growth in a PHP process, different situations were studied under isothermal conditions, as marked in Fig. 1a; these are (1) imprint at room temperature, (2) imprint at some mean temperature during heat-up, 80 °C, and (3) imprint at the targeted imprint temperature, 150 °C. These situations should disclose the effect of both external parameters, the pressure and the temperature on grain growth. To avoid any side-effect due to the differing heat-up history, we conducted these experiments as indicated in Fig. 1b. We skipped the heating process and loaded the imprint stack into the hot, pre-heated imprint system (‘hot loading’, HL) followed by unloading at the end of a specified imprint time. The pressure stays at 100 bar.

As the stamp, a piece of silicon (2×2 cm²) was used provided with an anti-sticking layer [34]; its surface energy is low, 10–15 mN/m. On purpose, the size of the sample was

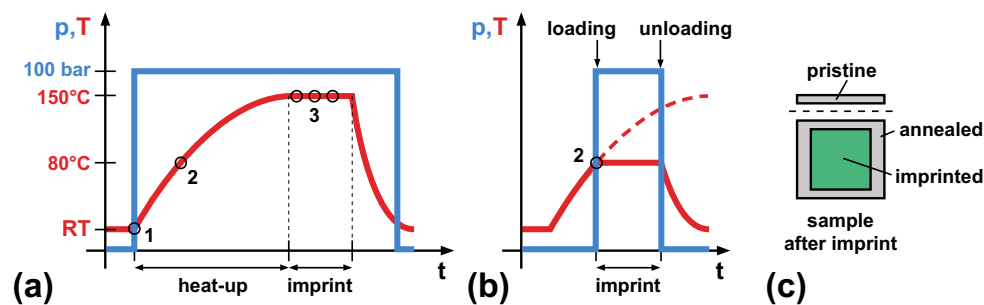


Fig. 1 a) Typical temperature and pressure characteristics against time for the PHP process ('planar hot pressing'). Temperatures under investigation are indicated by numbers (1–3). b) Temperature and pressure characteristics for a 'hot loading' (HL) process at a given

temperature to follow grain growth. c) Sample after imprint with imprinted (green) and annealed (grey) area, as well as piece cleaved from the sample for potential control of the pristine layer

larger than that of the stamp ($2.5 \times 2.5 \text{ cm}^2$), see Fig. 1c. This yields an imprinted and an annealed part allowing inspection of both situations with every sample. In view of the sample-to-sample variations observed, this is crucial to separate the effect of pressure and temperature on grain growth. To limit the exposure of the sample to ambient atmosphere, the imprint stack (heat conducting foil / sample / stamp / heat conducting foil) was wrapped into an Al foil (EN-AW1050A, 30 μm , Alujjet-Universal GmbH), forming a closed sachet [21]. The heat conducting foil (KU-CG30/R, 200 μm , Boyd Corporation GmbH) together with the Al represents a cushion that assures good contact to the press plates and a homogeneous pressure distribution during imprint. The sachet is prepared in ambient atmosphere. Beyond shielding the sample from free convection, its primary purpose for our experiments is to enable prompt loading at an elevated temperature, the key to experiments with short process times. With each sample, a strip about 5 mm wide was cleaved before imprinting to monitor the pristine layer.

The grain size was evaluated from scanning electron microscopy, SEM (S-FEG XL 30 S, Thermo Fisher Scientific). The inherent noise of the SEM micrographs prohibits an automated analysis of the grain size. Therefore, we measured the grain dimensions (approximate diameter D) manually using the software Fiji. All grains that were clearly identified from the micrographs were evaluated. Thus, very small grains may have been missed. The mean number of grains evaluated for a grain size distribution typically is at least 500 grains. Furthermore, the vertical grain orientation was characterized by XRD (X-ray diffraction) measurements (Bruker D2 Phaser) at room temperature ($\sim 25 \text{ }^\circ\text{C}$) within a scanning range of 10° to 60° 2θ , applying a step size of 0.02° and a step time of 0.05 s. The diffractometer was operated with a current of 10 mA, a voltage of 30 kV using a $\text{CuK}\alpha$ radiation source ($\lambda_{\text{CuK}\alpha 1} = 1.54059 \text{ \AA}$, $\lambda_{\text{CuK}\alpha 2} = 1.54449 \text{ \AA}$). Furthermore, AFM (atomic force microscopy) measurements (Bruker Innova System, tapping mode, tip: RTESPA-300; tip radius: $< 12 \text{ nm}$) were performed for selected samples.

3 Results and Discussion

3.1 Basis of investigation

The current investigation on grain growth with MAPbBr_3 layers starts by presenting the pristine layers used and their characteristics. State-of-the-art theoretical concepts represent the framework for establishing realistic expectations about the impact parameters relevant to grain growth of polycrystalline layers known from literature. Finally, the PHP process itself as performed with our specific thermal imprint system defines the experimental framework on hand to induce grain growth.

3.1.1 Pristine layer characteristics

To provide a well-funded basis for our investigation, we characterized the pristine layers used for the imprint experiments, as prepared by spin coating and soft bake at $125 \text{ }^\circ\text{C}$. These layers may contain some residual solvent (boiling point of DMF is $153 \text{ }^\circ\text{C}$) and, in addition, impurities from the acetate group [21]; the lead precursor used is the acetate $\text{Pb}(\text{Ac})_2$. SEM inspection indicates some waviness of the surface. A comprehensive impression is provided from a sample cross section, see Fig. 2a/b. In parts, the layer is quite compact; in other parts, it features hollows to the substrate interface. The latter looks as if the wavy surface represents a largely continuous 'crust' covering a loose bottom layer, featuring single more or less isolated crystallites. To test whether the apparent hollows exist at the cleaved front only we detached a part of the layer from the substrate by means of a gluing pad; Fig. 2c shows it from its bottom side. The crystals visible are cubic, as anticipated with MaPbBr_3 . Single large crystals are visible; the majority of the grains has dimensions in accord with the mean grain sizes evaluated from top view SEM micrographs, $\approx 200 \text{ nm}$. To a large amount, the grains at the interface to the Si substrate (covered with native oxide) feature a (100)-orientation, with

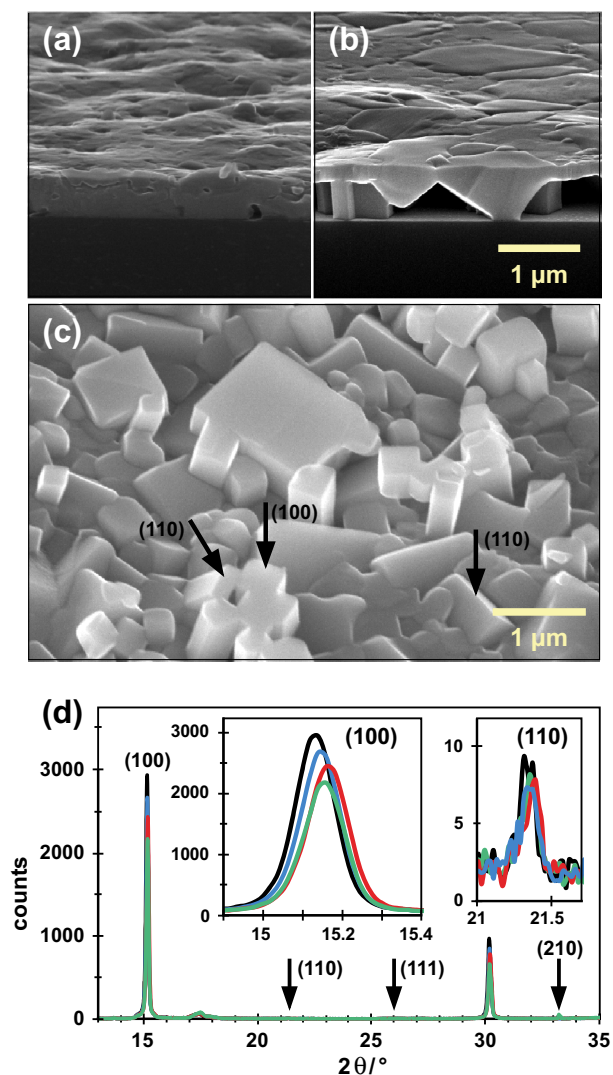


Fig. 2 Characteristics of the pristine layer used for imprint experiments (soft bake 125 °C, 2 min; mean initial grain size 170 nm). Locally differing morphology of the layer in cross section (a/b) and detached part of b) flipped around (c); XRD measurements (d) with different pristine layers from the same batch to indicate sample-to-sample variations. The two main peaks refer to the (100) and (200) orientation

some axial deviation. However, also some grains with rather a (110)-orientation are discernible (see inclination of almost 45° in Figs. 2b/c); we also found a few grains featuring a triangular interface geometry, indicative of a (111)-orientation. Characteristic XRD measurements taken from the surface are given in Fig. 2d; the diffraction pattern is dominated by the reflection of the (100) and (200) planes; the contributions of the (110) planes are only minor (see inset); (111) orientations seem to be below the limit of detection.

Figure 2a/b suggests that the nucleation of the perovskite occurs heterogeneously, starting from the substrate interface [37] and, in particular, from the free surface of the layer.

The latter may result from the interaction of the gradient of solvent induced by evaporation in combination with the temperature gradient during soft bake, increasing the solubility of the perovskite at the free surface; MaPbBr_3 features an inverse solubility [38].

The limited contact area with the substrate may account, among others, for the well-known deficient adhesion of perovskite layers on a Si substrate; for remedy substrate preparation commonly involves measures to increase adhesion; for instance, earlier experiments had shown that the exposure of the substrate with an excimer lamp to increase its surface energy is beneficial to provide continuous perovskite layers on Si (see Supporting Information, Fig. S-1). Already with MaPbI_3 , we found the contact of perovskite layers to the substrate to be limited [20], however, not as pronounced as with the current samples.

Revisiting the XRD measurements, Fig. 2d documents another issue less regarded so far when evaluating the results, sample-to-sample variations. The four samples shown here are chosen from the same batch (they were prepared in the same run from a single precursor solution). Obviously, intensities varying by up to about 20% and peak positions varying by up to 0.1° should not be interpreted. Similarly, the initial grain size varies somewhat; hence, the respective mean grain sizes of the pristine layers are denoted with the experiments depicted hereafter.

Moreover, the XRD results clearly show that all pristine layers primarily feature a (100)-orientation of the grains; differing textures were only minor (see arrows in Fig. 2d). We suggest that this is due to the primarily heterogeneous nucleation from the substrate interface and the free surface. In fact, heterogeneous nucleation at the substrate is reported as being typical of perovskite layers spin-coated from a precursor solution [14]. In view of nucleation and growth, it means that the (100) orientated crystals of the perovskite crystal provide both, a surface free energy and an interface energy to the substrate that are low. From theory [13], it is well known that the (100)-planes of a MAPbBr_3 crystal feature the lowest surface energy, a factor of 6–8 smaller than with a (110)- or (111)-orientation. Calculated values amount to 64–128 mN/m [13], depending on surface termination. Thus, a (100)-orientation at the free surface holds the contribution of the film surface to the overall energy of the grain small. The substrate interface benefits even more in this respect; with a minimum surface energy of 64 mN/m of the perovskite and a comparable surface energy of the substrate of 60–70 mN/m [34], the interface energy is very small (– it vanishes with $\gamma_{s0} \approx \gamma_{sub}$ –), so that the contribution of the bottom interface to the grain energy should be negligible, even when the real values of γ_{s0} for the perovskite differ somewhat from the calculated ones (– due to the polarity of the compound γ_{s0} will be high). A low surface energy and a negligible interface energy with a particular orientation (100) are of outstanding benefit to the formation of columnar

grains spanning the whole layer thickness. We will address the consequences of the orientation of the pristine layer in detail in Sect. 3.2.

3.1.2 Fundamentals

Grain growth in polycrystalline materials has been addressed with diverse objectives. The basic concepts were developed with metals, where processing by hot and cold forming in combination with annealing is determinant in tuning their mechanical properties [39, 40]. With a transfer of these concepts to classical semiconductors (Si, Ge), the attention focussed on the morphology dependence of the electrical properties [4, 6, 10, 11], where advances of microelectronics draw the interest on grain growth in thin layers on a substrate, with semiconductors and metals as well [16, 28, 41, 42]. Recently, grain growth with emerging organic or hybrid compounds has set a new focus on e.g. optical properties and their correlation with layer morphology [12, 14]. In particular with hybrid metal halide perovskites, it has become evident that large-grained layers are mandatory for high-quality devices [12, 23, 43]. Most often large grains are achieved by inducing grain growth in a post-processing step [15, 17, 44]. When currently the post-processing step with perovskites is imprint, the mechanical properties related with grain growth are of concern during preparation.

Basically, grain growth in a polycrystalline system serves to reduce the overall internal energy related with grain boundaries, γ_{gb} characterizing their energy per area. The relative grain boundary area (per volume) is reduced by decreasing the curvature of the grain boundaries, resulting in capillary-driven grain growth; the mean (equivalent) grain radius \bar{r} increases. With pure materials, the capillary-driven growth rate follows [1, 16]

$$\frac{d\bar{r}}{dt} \propto M(T) \cdot \gamma_{gb} \cdot \bar{\kappa} \tag{1}$$

with M the grain boundary mobility featuring an Arrhenius-type of temperature behaviour, $M(T) = M_0 \exp(-Q_n/kT)$, Q_n being the activation energy for grain boundary motion; M_0 is a material-specific constant. With spherical grains in the bulk of a material, the mean curvature $\bar{\kappa}$ can be identified with $1/\bar{r}$, resulting in an isothermal growth law of $\bar{r}^2 \propto t$, or $\bar{r} \propto t^{1/2}$, for the so-called normal growth [1, 28]. In praxis, the temporal evolution may differ from this ‘ideal’ case and growth is generally described as $\bar{r} \propto t^{1/n}$, or more precisely (including the initial radius \bar{r}_0) according to [16, 41]

$$\bar{r}^n - \bar{r}_0^n \propto M_0 \cdot \exp\left(-\frac{Q_n}{kT}\right) \cdot t \tag{2}$$

with the growth exponent n differing from the ideal value of 2. Thus, with isothermal processing ($M = const$) the time evolution of grain growth is mainly independent from

temperature. (Of course, Eq. (2) has to be regarded as a numerical relation due to the unspecified value of n ; only with $n = 2$ it represents a physical relationship.) Compared to ‘normal’ growth, pure ‘secondary’ growth is fast; the respective growth exponent amounts to $n = 1$ [26, 28, 45]. Otherwise, a value of $n \approx 3$ is reported with doped semiconductors [46] and also with the growth of non-equiaxed grains as typical of growth during deposition [19]. Though in praxis the growth exponent n may vary, the idealized situation with $n = 2$ is fully adequate for a basic assessment.

Normal grain growth with time ($n = 2, \bar{r}_0 = 0$) is visualized in Fig. 3, giving a linear plot (a) and, in addition, a double-log plot (b) over a somewhat wider range. Different curves refer to different temperatures; the activation energy is taken from perovskite literature, $Q_n = 0.76\text{eV}$ for normal growth [12]. The temperature range mirrors typical perovskite processing;

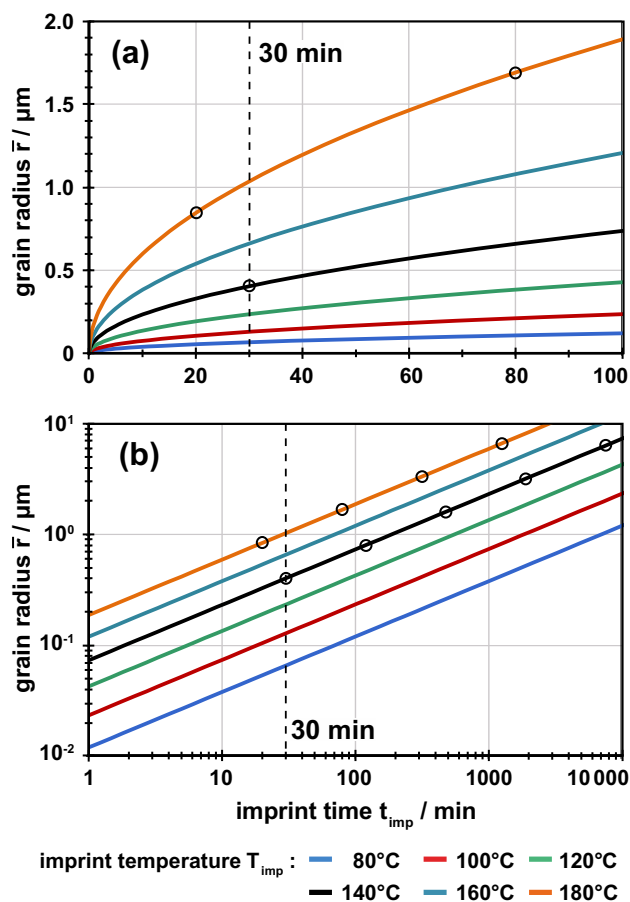


Fig. 3 Grain growth according to Eq. (2), with $\bar{r}_0 = 0, n = 2$ and $Q_n = 0.76\text{eV}$; the curves refer to temperatures of 80 °C to 180 °C in steps of 20 °C. a) Linear plot, b) double-log plot to indicate the growth behaviour over a wide span of times and grain sizes. (Dots mark a doubling of the grain radius). With an initial grain radius $\bar{r}_0 \neq 0$, the curves follow the simple exponential behaviour with longer times only, the regime of smaller times will be dominated by \bar{r}_0

similarly, the range of grain sizes is typical, from 100 nm to some micrometres.

Starting with a certain initial grain size, $\bar{r}_0 \neq 0$ will overwrite the curves at short times. Only when $\bar{r}^n \gg \bar{r}_0^n$ the initial grain size can safely be ignored. Based on a tolerance of 10%, this is the case with $\bar{r} \geq (10)^{1/n} \bar{r}_0$. In praxis, \bar{r}_0 may not be negligible. We will re-address this practical issue in Sect. 3.2.1 in context with thermal annealing and in Sect. 3.3 with respect to the evaluation of n from PHP experiments.

Figure 3 points to a number of practical implications from the growth law. (i) Growth is fast initially but slows down with time; doubling the grain size at $T = \text{const}$ requires a fourfold time with $n=2$ (see dots in Fig. 3). This raises the question of the significance of a time increase to achieve a targeted grain size. (ii) Treatment temperature accelerates growth substantially; this raises the question of the choice of the processing temperature in view of an achievable grain size within a realistic time span. (iii) With the growth law according to Eq. (2), the growth exponent n stays similar with any temperature chosen (temperature affects the grain boundary mobility M only); this raises the question whether such a constant growth exponent matches the behaviour of the material studied here, MAPbBr₃. (iv) Similar to an increase in temperature, an increase in the material-specific pre-factor M_0 or a decrease in the activation energy Q_n shifts the curves upwards; this raises the question as to what determines the value of M_0 and Q_n , or rather whether it is possible to improve these parameters.

Whereas the issues (iii) and (iv) will be addressed later, it is viable to draw consequences from (i) and (ii) for the design of meaningful grain growth experiments right now. In praxis, the processing time allowed will be limited; let us assume a maximum time of 30 min as an example, as marked in Fig. 3. Within this time, the grain size achievable is highest with the highest temperature; a compensation of temperature reduction by an increase in treatment time seems less reasonable, particularly as the growth rate decreases with time (with $n > 1$). Thus, the highest temperature possible is the best choice for efficient grain growth. Of course, other issues may limit the processing temperature. For instance, it may be the system used for post-treatment. In case of perovskites, it is most often a physical issue, thermal decomposition. With our material, a temperature of 150 °C had shown efficient grain growth along with negligible degradation under imprint conditions [21]; thus, we stay with this temperature for the current investigation. This temperature choice enables the design of convincing experiments; in view of grain growth, Fig. 3 suggests that temperatures as low as 80 °C–100 °C may be less effective to induce substantial grain growth with hybrid metal halide perovskites, in accord with the literature [44, 47, 48].

3.1.3 PHP process

As already stated, the current investigation aims at understanding the post-processing results obtained with MAPbBr₃ via ‘planar hot pressing’ (PHP, see Fig. 1a), i.e. imprint with a flat stamp to induce grain growth. Though simple in view of the procedure—a constant pressure of 100 bar is operative during the whole imprint process—it is complex in view of grain growth. As typical of plate-based imprint systems, the heat-up phase is long when a high temperature has to be reached; in our system it takes about 20 min to heat the plates to 150 °C, our processing temperature (see Fig. S-2, Supporting Information). During this period, grains already grow, however, at a dynamically increasing temperature and hence an increasing grain boundary mobility and growth rate. Merely the ‘real’ imprint phase of typically 5 min works at almost constant temperature and thus a constant mobility.

With regard to grain growth, the PHP process lends itself to separate the heat-up phase from the imprint phase in a first step. Figure 4 documents this approach; part a) exhibits grains after the heat-up, part b) after an additional imprint of 5 min. The grain sizes obtained do not differ substantially with or without the imprint phase. As with both cases, the layers were very flat; we degraded the surface in the SEM by electron beam irradiation with the purpose to ‘mark’ the grain boundaries for later evaluation; Fig. 4 shows the initial surface and the degraded surface, with both situations. By doing so, the evaluation of a mean grain size (from about 400—500 grains) was substantially simplified.

Evaluation of the grain size indicates that in fact some growth occurred during the imprint phase. At the end of the heat-up phase, the mean grain size was as high as 570 nm (mean initial grain size: 170 nm); after an additional imprint of 5 min, it just increased to 610 nm. This emphasizes the dominance of the heat-up phase with grain growth via PHP with short imprint times, here 5 min. Qualitatively, it can be related to the growth rate at constant temperature being high at the beginning but slowing down afterwards.

However, a PHP process is not ideal for investigating grain growth; with short PHP times, the dynamic increase in the grain boundary mobility during heat-up represents a specific uncertainty. Therefore, we investigate grain growth by means of a ‘hot loading’ process as presented in the next paragraph. We will re-address our PHP results in context with theory in Sect. 3.2.6.

3.2 Identification of impact parameters

To identify the involvement of the two external processing parameters p_{imp} and T_{imp} in grain growth with MAPbBr₃, isothermal experiments were performed under ‘hot loading’ (HL) conditions (Fig. 1b). The three situations investigated

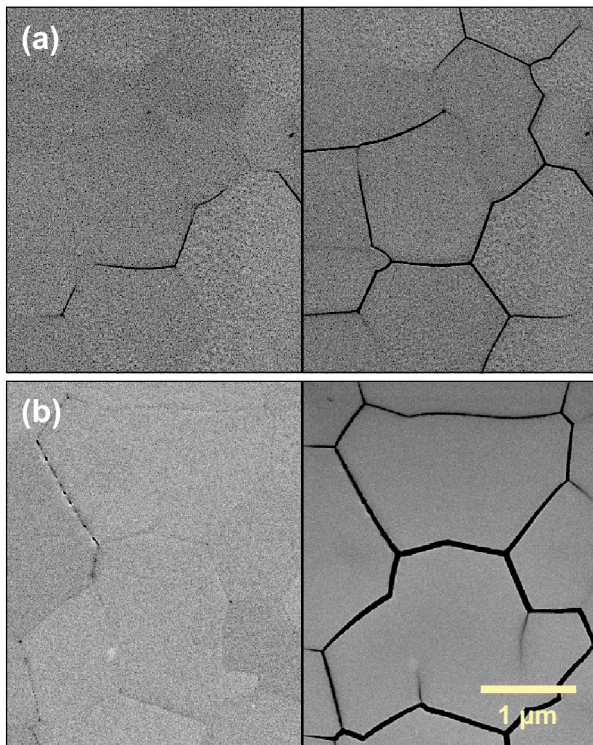


Fig. 4 Typical micrographs documenting grains grown in a PHP process at 150 °C (soft bake 125 °C, 2 min; mean initial grain size 170 nm). **a** After the heat-up phase, mean grain size 570 nm. **b** After an additional imprint of 5 min (complete PHP process), mean grain size 610 nm. Left: proper surface with flat grains; right: similar surface after about 30–60 s of e-beam irradiation to visualize the grain boundaries (acceleration voltage $V_{acc}=20$ kV, inspection: spot size 2 nm, degradation: spot size 4–6 nm)

refer to three different temperatures, see Fig. 1a, (1) room temperature (RT), (2) some medium temperature during heat-up (80 °C) and (3) the targeted imprint temperature (150 °C). In view of Fig. 3, the choice of 80 °C seems low. But this temperature was chosen deliberately as any grain growth due to temperature alone should be negligible; however, it may be the case that in combination with the applied pressure of 100 bar the mobility of the grain boundaries is sufficient to induce growth. Moreover, 80 °C is a critical temperature with respect to the long-term stability of perovskite-based photovoltaics, however, without the additional pressure.

To catch grain growth as early as possible, loading and pressure application were optimized to enable short isothermal imprint times. The loading of the stamp/sample assembly (sachet wrapped in Al foil, see Experimental) to the pre-heated press takes less than 5 s; subsequent pressure application runs automatically and takes another 3 s to move the plates into contact at the designated pressure; the movement is performed in a single step provided by a pre-adjustment of the plate movement required to attain

the targeted pressure level, a feature enabled by the stepper motor combined with the piezo-control of the imprint system used [35]. The shortest imprint time with HL (counting from the moment when full pressure is applied) achieved reproducibly is 10 s (± 1 s).

Then, the evaluation of the ‘imprinted’ and just ‘annealed’ part of each sample (Fig. 1c) is the key to distinguish the effect of pressure from that of temperature when both factors are operative. To compare with the grain growth in a conventional situation, far from imprint, thermal annealing at 150 °C was used as a reference experiment. Grain growth with time was followed by evaluating SEM micrographs, along with XRD measurements to indicate grain orientation. To minimize flawed implications, the experiments were performed under subtle control. Within one experimental run, samples prepared from the same batch were used preferably; when necessary, the ‘starting conditions’ could be tracked by checking the status of the pristine layer with each data point from a slice retained (Fig. 1c).

3.2.1 Reference experiment

Figure 5 summarizes the results obtained with thermal annealing at 150 °C in a nitrogen atmosphere, our reference. To monitor grain growth over a wide range, the soft bake was performed at 75 °C for this set of experiments; as a consequence, the mean grain size before annealing was low. Grain growth was characterized with samples annealed for 10 s up to 30 min on a hotplate; the layer thickness was $h \approx 370$ nm.

Figure 5 a) starts with typical SEM micrographs after 1 min and 30 min of annealing, indicating substantial grain growth with time. The mean diameter D_m of the grains increases from 90 nm (pristine) to 280 nm (1 min) and 810 nm (30 min). Figure 5 b/c) gives the respective grain size distributions. With both situations, the grain size is well characterized by a log-normal course (see continuous line), in accord with the literature [16]; this similarly holds with all annealing times. Thus, grain growth proceeds in a self-similar way; when plotted logarithmically, it can be described by a normal distribution of almost constant width (logarithmic standard deviation $LSD \approx \text{const.}$), as demonstrated in Fig. 5 d); for clarity only the two selected distributions together with one of the pristine layer are shown. Further information on the distributions evaluated is given in the Supporting Information, Fig. S-3. XRD demonstrates that the orientation of the grains stays similar during growth and remains similar to one of the pristine layer (Supporting Information, Fig. S-4). Thanks to the nitrogen atmosphere, any peaks indicating degradation were not observed.

The mean grain size follows a growth law according to $D_m \propto t^{1/n}$, see Fig. 5e. It is well characterized by a slope of ≈ 0.35 over the whole annealing period, without any

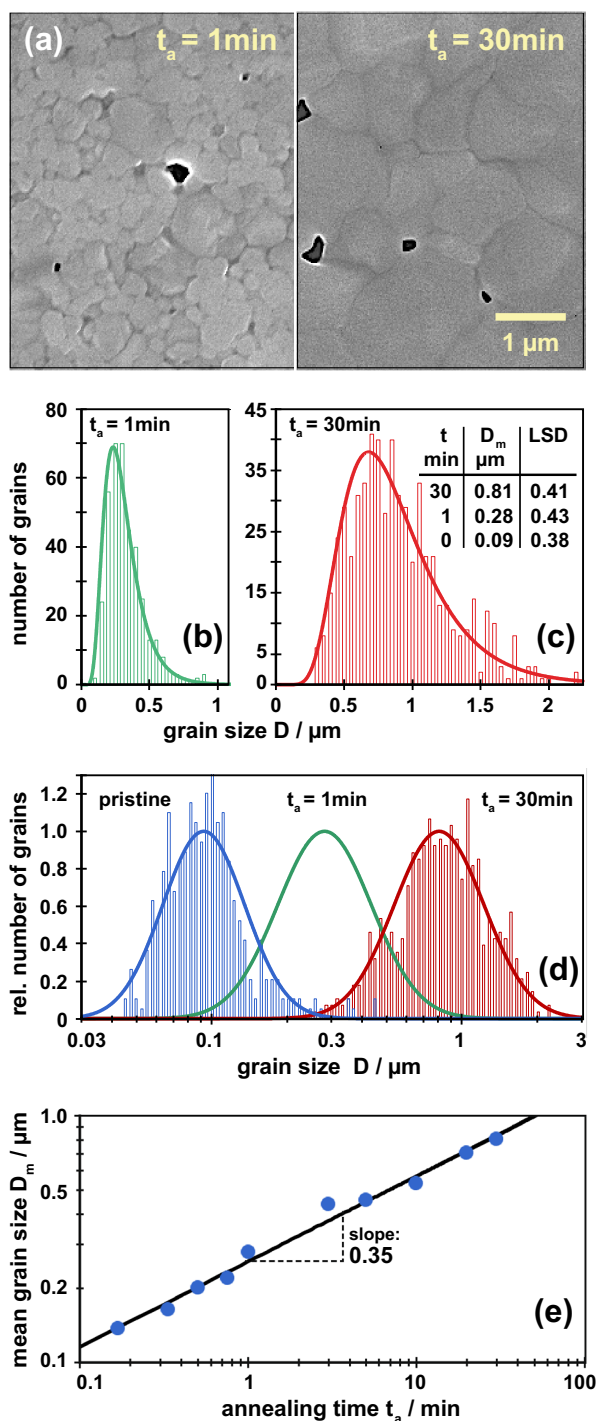


Fig. 5 Grain growth under temperature only (control experiment); annealing at 150 °C in nitrogen (soft bake 75 °C, 2 min; mean initial grain size 90 nm). **a** SEM micrographs as typical of annealing times of 1 min and 30 min. **b/c** Grain sizes evaluated with 1 min and 30 min annealing, indicating a log-normal distribution. (The curves given are calculated from the experimental characteristics, the mean grain size D_m and the respective logarithmic standard deviation, LSD. **d** Self-similar growth of the grains as documented by a normal distribution of constant width when plotted on a logarithmic scale (data for pristine layer and 30 min HL only.). **e** Evolution of mean grain size with time; the log–log plot indicates an exponential growth with an overall slope of 0.35 ($n_{est} = 2.89$, see text). Evaluation from $D_m > 2D_0$ on results in a slope of 0.33 ($n = 2.99$)

indication of a change in growth behaviour. As already addressed at the end of Sect. 3.1.2, a precise evaluation of n requires to consider the grain size D_0 that exists prior to annealing, dominating the initial growth phase. With $n \approx 3$ (our experiment), grain sizes of $D_m > 2D_0$ follow the exponential law $D_m \propto t^{1/n}$ with an accuracy of at least 10%; Fig. S-5 in the Supporting Information shows this graphically. Simply evaluating all data points (including the initial growth phase) may already result in a good estimate of the growth exponent for praxis (see Sect. 3.3), here $n_{est} = 2.89$; with the experiments hereinafter, we give both values, n and n_{est} . With N_2 -anneal, their difference is small and the growth law is well characterized by an exponent of $n \approx 3$.

The result obtained implies that general literature concepts ask for some reassessment with perovskites. The growth law observed ($n \approx 3$) does not comply with a classification of growth into ‘normal’ ($n \approx 2$, bulk-dominated, random grain orientation) and ‘abnormal’ or ‘secondary’ growth ($n \approx 1$, surface-dominated, development of preferential grain orientation). Already with classical semiconductors, it was remarked that “grain growth in thin films is rarely, if ever, normal” [28]. Such reservations are ascribed to the fact that with semiconductor films growth occurred already during deposition, not just afterwards (as with almost amorphous metal films); typically, columnar grains with diameters that are small compared to the layer thickness evolve, due to heterogeneous nucleation at the substrate and growth in vertical direction. A similar situation exists with the solution-grown perovskites as documented in the preceding paragraph; already the pristine layers feature a clear (100)-texture, pointing to the impact of the surface/interface energy during the nucleation of the perovskite grains (Fig. 2d). Thus, with our perovskite layers the free surface and the substrate interface did already dominate the process of layer formation, before thermal annealing. Under these premises, the grains are already oriented with their favourable (100)-orientation perpendicular to the substrate; bulk-dominated ‘normal’ growth of grains with random orientation will not occur at any time of the coarsening process. Similar to nucleation, grain growth with perovskites is surface-dominated. However, it cannot be identified with ‘secondary’ growth in its original terms; the growth exponent is far from $n \approx 1$ and growth is not accompanied by the development of a preferential orientation out of grains with random orientation.

Though a ‘normal’ or ‘secondary’ growth is not characteristic of our perovskite layers the growth law, Eq. (2), describes grain coarsening quite well, here with $n \approx 3$. This growth exponent is well in accord with the literature on layers with heterogeneous nucleation at the substrate [19] or with layers containing impurities [46]; the latter may be expected with the acetate-based Pb-precursor used [21].

Furthermore, in contrast with the literature [49] there is no indication of a stagnation of growth within the time span investigated. The reason may be that stagnation was not yet reached with our experiments after 30 min, with mean grain sizes of ≈ 810 nm (the layer thickness is about 370 nm). With stagnation due to surface grooving, the factor between D_m and h scales with the ratio of surface energy to grain boundary energy according to $D_m/h \approx 2\gamma_{s0}/\gamma_{gb}$ [29]. In fact, with $D_m/h \approx 2.2$ (our experiment) stagnation is not expected as long as $\gamma_{s0}/\gamma_{gb} > 1.1$; according to physical expectation, grain boundary energies should be substantially smaller than surface energies of crystals as their number of open bonds is smaller. With $\gamma_{s0}/\gamma_{gb} = 2 - 3$ [30], grooving-induced stagnation could be expected for $D_m/h > 4$, here with grain sizes of $D_m \geq 1.5 \mu\text{m}$.

We will re-address stagnation with a long-term experiment at 150 °C under HL conditions in Sect. 3.2.4 as well as in context with impurities in Sect. 3.2.7. Stagnation is still denoted as one of the unresolved issues with grain growth [50].

3.2.2 Imprint at RT

To characterize the impact of pure pressure on grain growth (position ‘1’ in Fig. 1a), two types of experiments were performed, a variation in the pressure ($p = 10$ bar to 100 bar) at a fixed time of 5 min and a variation in the treatment time ($t = 10$ s to 5 min) at a fixed pressure of 100 bar. The soft bake temperature was 125 °C as with all imprint experiments, with a mean initial grain size of about 200 nm in the pristine layers.

On the whole, the experiments at RT did not reveal any clear impact of the pressure. Though SEM inspection could identify locally flattened parts of the surface (see Supporting Information Fig. S-6), neither a densification of the layer nor a grain growth was identified. AFM measurements (see Supporting Information Fig. S-7) indicate a roughness that is comparable to that of the respective pristine layers. (Earlier experiments performed with pristine layers soft baked at 75 °C had shown a densification of the layer but no grain growth, however, with a trihydrate-based precursor, see Supporting Information Fig. S-8.) Similarly, XRD measurements did not reveal a significant change due to pressure only (see Supporting Information Fig. S-9); neither the slight shift in peak position nor the slight change in peak intensity was systematic; all changes observed were in the range of the sample-to-sample variations already addressed in Fig. 2d.

From these results, we have to conclude that without any heating the elastic energy that is provided to the perovskite layer in a typical imprint process is too low to induce grain growth; this issue is addressed in Sect. 3.2.5. The literature has demonstrated a deformation of the MAPbBr_3 crystal and

a phase transformation induced by pressure at RT, yet in a pressure range far beyond the one of imprint (4–120 kbar) [51]. However, even at these high pressure levels the changes induced were fully reversible and did not result in plastic deformation; grain sizes were not reported.

With MAPbBr_3 layers, we have to conclude that a pure pressure (up to 100 bar) is not effective to induce grain growth.

3.2.3 Imprint at 80 °C

During the heat-up phase of PHP, growth occurs (see Fig. 4a); however, not the complete heat-up time will be relevant. For instance, at 80 °C pure thermal growth is negligible though the grain boundary mobility is increased compared to RT. With the HL experiment in position ‘2’ (see Fig. 1a/b), the question is whether the pressure during imprint makes a difference. More precisely, whether a temperature as low as 80 °C in combination with a typical imprint pressure (100 bar) is able to induce grain growth in our perovskite.

Albeit the treatment time was varied over a wide range (10 s to 60 min), the experiments could not show a distinct effect of pressure in combination with temperature on grain growth at 80 °C. The mean grain size remains at the value found with the pristine layer, ≈ 200 nm. Typical results obtained after 30 min of HL at 80 °C are given in Fig. 6; part a) and b) give cross-sectional views of the layer, referring to the ‘imprinted’ and the ‘annealed’ part of the sample, respectively (see Fig. 1c). The annealed part (Fig. 6b) looks similar to the pristine layer, see Fig. 2b, with the characteristic hollows observed. The imprinted part (Fig. 6a) features some local flattening of the surface; however, pre-existing hollows still remain. Corresponding XRD measurements (Fig. 6c) provide evidence that the crystallinity was not changed; neither with the main (100)-peak nor with the minor (110)-peak a clear effect of the HL at 80 °C can be verified; again the changes are in the range of the sample-to-sample variations.

It has to be stated that the imprint pressure seems to be without effect to induce grain growth at temperatures too low to induce pure thermal growth. With substantially higher pressures (2 kbar) and a somewhat higher temperature (90 °C), the literature [52] reports compaction of MAPbI_3 layers and an improved coverage (– due to its mechanical properties [53] this material should require lower pressures to deform than MAPbBr_3), however, without addressing grain growth. Furthermore, pressing at 100 °C resulted in flattened layers with reduced pinholes, though the pressure was as low as 5 bar; however, again grain growth was not observed [44]. Even in a non-hydrostatic experiment (being near to the imprint situation) pressure is effective only when in the kbar-range [54]. Though the material and

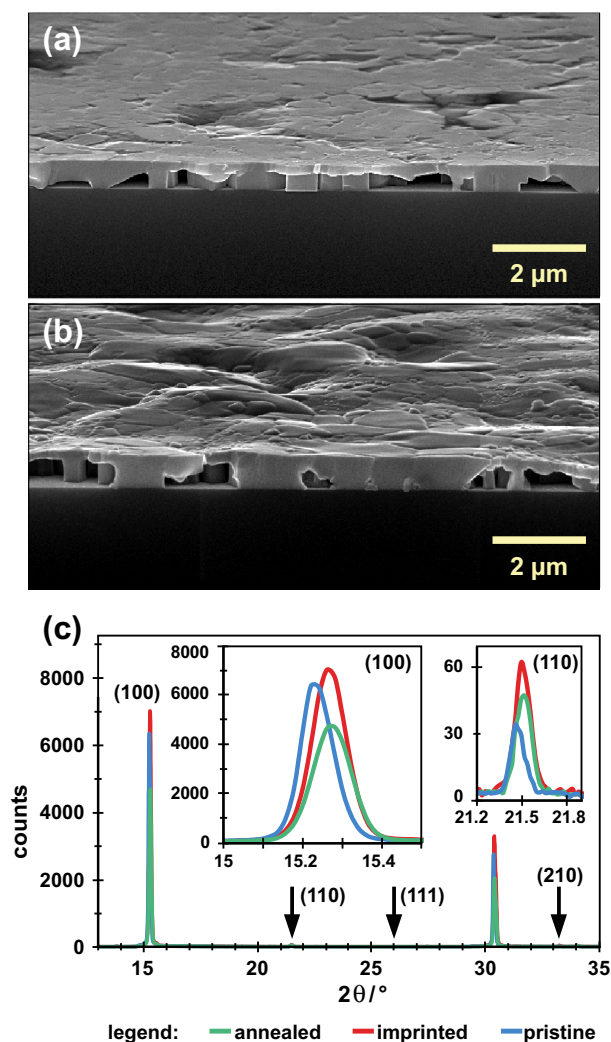


Fig. 6 HL experiment at 80 °C for 30 min (soft bake 125 °C, 2 min; mean initial grain size 170 nm). The SEM cross sections give typical situations with the ‘imprinted’ part (a) and the ‘annealed’ part (b) of the sample. The XRD measurement (c) refers to both regions and compares with the measurement of the respective pristine layer (green: ‘annealed’, red: ‘imprinted’, blue: pristine)

the processing conditions of these references preclude direct comparison, we suppose that with PHP the temperature range up to 80 °C can safely be ignored with respect to grain growth in MAPbBr₃.

3.2.4 Imprint at 150 °C

Compared to 80 °C, there is a distinct increase in grain size when hot loading is performed at 150 °C (position ‘3’ in Fig. 1a). Grain sizes were evaluated for HL times of 30 s up to 30 min, a range similar to the annealing experiments under nitrogen (Fig. 4). Additionally, a long-term experiment was performed, with an imprint time of one day. Though a treatment of one day is not realistic in praxis, it

helps to clarify the physical question of a potential stagnation of grain growth, as addressed before.

The main results are summarized in Fig. 7; part a) displays corresponding situations within the ‘annealed’ part (no pressure) and the ‘imprinted’ part (pressure 100 bar) of a sample, part b) gives the respective grain size distribution, part c) documents the increase in the mean grain diameter with time, and part d) shows the logarithmic standard deviation (LSD) of the respective grain size distributions. To differentiate the effect of pressure and temperature, the grain sizes were evaluated separately in the ‘imprinted’ part (pressure and temperature) and in the ‘annealed’ part (temperature only), see Fig. 1c.

With both parts, the ‘imprinted’ and the ‘annealed’ part as well, the growth law according to Eq. (2) characterizes grain coarsening in an adequate way, indicated by the two overall regression lines in the double-log plot of Fig. 7c. The growth exponent amounts to $n_{est} = 3.8$ (slope 0.26) in the ‘imprinted’ part but is substantially higher, $n_{est} = 9$ (slope 0.11), in the ‘annealed’ part. In both parts, the grain size follows a log-normal distribution; the respective logarithmic standard deviations (see Fig. 7d) do not feature any trend but stay largely constant ($LSD = 0.4$), implying self-similar growth. The example for the grain size distribution in Fig. 7b refers to the ‘imprinted’ part of the long-term experiment. The grain size distributions for all imprint times are given in the Supporting Information; the distributions for the ‘annealed’ parts look qualitatively similar (see Fig. S-10) to the distributions for the ‘imprinted’ parts (see Fig. S-11).

With short HL times (below 1 min), the grains are of similar size in both parts; this may document a similar starting condition within the sachet. With ongoing time, the grains in the ‘annealed’ part develop a distinct difference to those in the ‘imprinted’ part, with a significantly smaller grain size. To assess whether this slope difference is due to degradation, XRD measurements were performed (see Fig. S-12, Supporting Information)—the sample in the sachet may feature a water film on its surface due to assembly in atmosphere. However, the PbBr₂ signal characteristic of the respective degradation product is not significant; moreover, it is higher with the ‘imprinted’ than with the ‘annealed’ part. In case that these small differences are to be valued, they may be understood from the fact that the stamp retains the water film (diffusing in and inducing some degradation in the ‘imprinted’ part), whereas partial evaporation from the surface into the sachet may reduce in-diffusion and water-induced degradation in the ‘annealed’ part.

Interestingly, though the layer in the ‘annealed’ part looks disrupted (see Fig. 7a), the grains still existing are clearly assigned to the MAPbBr₃ perovskite, albeit with a significantly reduced intensity of the main (100)-peak (XRD, Fig. S-12, Supporting Information). We suppose that the effect leading to the morphology of Fig. 7a is a general one, the

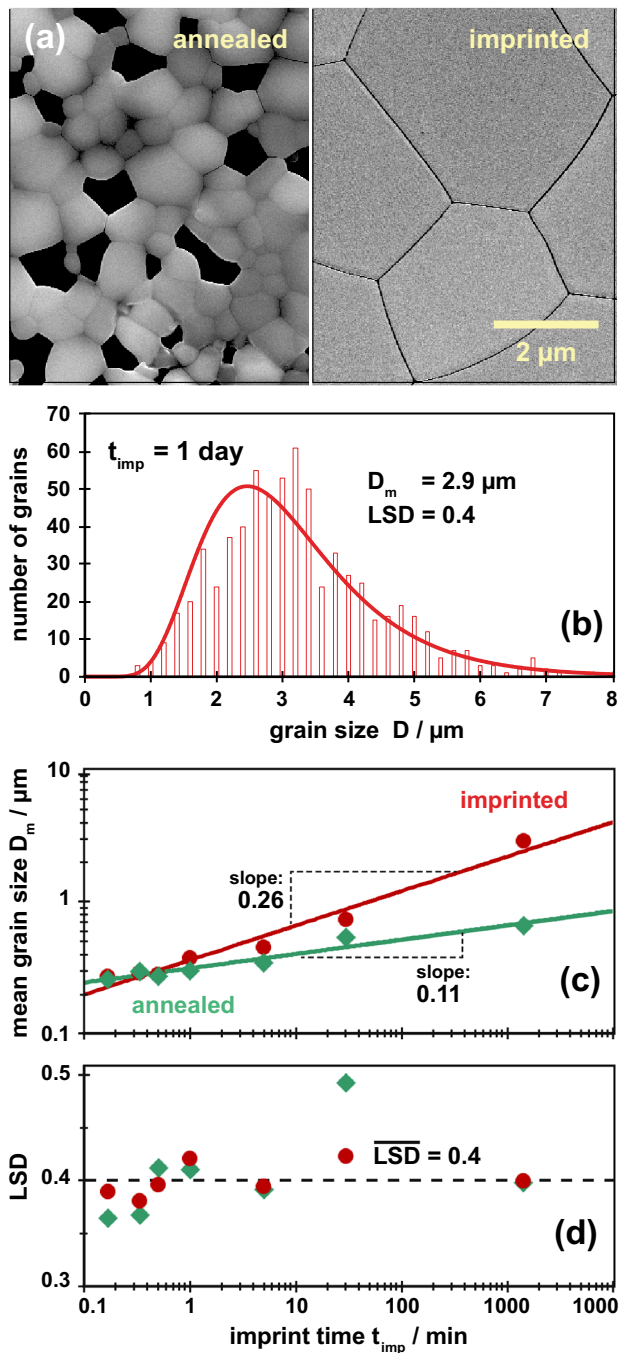


Fig. 7 HL experiment at 150 °C. The treatment time was varied from 30 s to 1 day. The data refer to samples from two different batches, batch (1): $t \leq 1 \text{ min}$ and batch (2) $t > 1 \text{ min}$. (Soft bake 125 °C, 2 min; mean initial grain size 150 nm (1) and 170 nm (2). **a** Typical morphology after 1 day of HL within the ‘annealed’ part and the ‘imprinted’ part of the sample. **b** Log-normal grain size distribution for the long-term experiment (1 day). **c** Increase in mean grain size with time for the ‘imprinted’ and ‘annealed’ part of the sample, overall slopes 0.26 ($n_{est} = 3.82$) and 0.11 ($n_{est} = 9.22$) in the imprinted part (with pressure) and the ‘annealed’ part (without pressure), respectively. Evaluation from $D_m > 2D_0$ results in $n = 3.43$ and 8.92, respectively. **d** Logarithmic standard deviations of the grain size distributions

instability of thin, polycrystalline films during annealing as e.g. similarly observed with metals and ceramics [55]. When a thin polycrystalline layer is annealed, grooves develop at positions where grain boundaries meet the free surface of the layer, a consequence of developing a local force balance between surface energy (γ_{s0}) and grain boundary energy (γ_{gb}). As long as grain growth is fast, the grooves are faint and become dragged along during movement of the grain boundaries [30]. However, with large grains the movement of the grain boundaries slows down with time (see growth law Eq. (2), Fig. 2a) and the grooves become deeper (– the diffusion of atoms enabled by the rate of thermal energy supply feeds two competing mechanisms, grain boundary movement and grain boundary grooving as well). With thin films, when the grooves reach the substrate, holes develop at grain boundary junctions first, followed by a complete separation of single grains in a later stage. The atomic diffusion process during this ‘over-annealing’ [56] transforms a flat, coherent polycrystalline layer (when thin enough) into separated bulky grains [55]. This process is well suited to explain the morphology of Fig. 7a in consideration of the XRD result. In contrast, within the ‘imprinted’ part of the sample the stamp restricts any atomic rearrangement near the grain boundaries in three dimensions and holds the layer flat, thus suppressing grooving.

As explicitly pinpointed in Fig. 7c, even the long-term experiment with 1 day of HL (1620 min) is well covered by the growth law with a constant growth exponent n . Against expectations, no stagnation of grain growth could be identified. After 1 day of HL, the mean grain diameter reached is $D_m \approx 3 \mu\text{m}$; the grains are about a factor of 8 larger than the layer thickness ($h \approx 370 \text{ nm}$). When grooving is in fact the reason for stagnation [29] (as it may occur at the free surface during N_2 -anneal), the lack of stagnation suggests that with HL the stamp actively promotes the formation of large grains by precluding surface grooving. Then, the pressure required for flattening the layer gains further significance for grain growth, beyond the one to diminish degradation at high temperature (as demonstrated earlier [21]).

Comparing grain growth in the ‘imprinted’ part under HL (Fig. 7c) with that under N_2 -anneal (Fig. 5e) provides further insight (for direct comparison see Fig. S-13a, Supporting Information). The slightly reduced overall growth rate (slope 0.26) compared to N_2 -annealing (slope 0.35) may result from some degradation as addressed above. Independent thereof the grain size obtained at long times is largely similar with HL and N_2 -annealing. However, with short times the grain size is higher with HL than with N_2 -annealing; after a first ‘jump’ the grains grow in a moderate way (for details see Supporting Information, Fig. S-13b), approaching the stationary regime for $t > 1 \text{ min}$. Of course, the larger grain size at short times results from the larger initial grains ($D_0 \approx 150 \text{ nm}$, due to the higher soft bake temperature);

yet, its somewhat abrupt increase (being similar with the ‘imprinted’ and ‘annealed’ part) may arise from the specific situation with the HL experiments; namely, it may be caused by some solvent within the sachet (a 2 min soft bake at 125 °C does not evaporate all DMF from the layer [21]); grain growth via solvent anneal from residual DMF is for instance reported at a temperature as low as 100 °C [57]. Though grain growth in the initial phase may differ with different techniques used, the stationary phase is highly comparable. We suppose that stationary growth is temperature driven and thus mainly independent from the process chosen, thermal imprint or N₂-anneal.

3.2.5 Role of stress

Stress is addressed in the literature as a driver for secondary grain growth [17, 29]. Under imprint conditions, three types of stress may occur in the layer, (i) a tensile stress due to grain growth, (ii) a compressive stress due to the pressure applied and (iii) a thermal stress, again compressive when T_{imp} is the highest temperature the sample meets during preparation. From the overall stress a driving force F_σ can be derived to characterize its impact.

The tensile stress in the layer due to grain growth, σ_{gr} , is always present; with columnar grains it results from the compaction of the layer, due to a transformation of less-ordered and less-dense material (the grain boundaries) into highly ordered and dense crystalline grains [29]. The respective stress depends on the relative amount of less-dense material and is quantified by Δa , the excess volume per area related with the grain boundaries; with metals, a value of $\Delta a \approx 0.1nm$ is reasonable [29]. Taking E^* as the biaxial Young’s modulus, this stress amounts to $\sigma_{gr} = E^* \Delta a (D_0^{-1} - D_m^{-1})$; it increases with grain growth. Its maximum value is related to D_0 ; taking modulus values after Feng [58, 59] (with (100)-orientation $E_{100}^* \approx 54GPa$) this results in $\sigma_{gr,max} \approx 50MPa$ for $D_0 = 100nm$ when the layer is stress-free at D_0 , namely $\sigma_{gr}(D_m = D_0) = 0$.

The stress in the layer due to the imprint pressure applied, σ_p , is compressive. Loading the sample with pressure in vertical direction results in an equi-biaxial stress in lateral direction as the layer is not allowed to expand. Assuming a Poisson’s ratio of $\nu \equiv \nu_{100} \approx 0.2$ [58, 60], this stress amounts to $\sigma_p = p_{imp} \cdot \nu / (1 - \nu) \approx 2.5MPa$ at an imprint pressure of 100 bar.

The thermal stress in the layer, σ_{th} , results from the difference in thermal expansion of the perovskite compared to the substrate. In our case, due to the low coefficient of thermal expansion (CTE) of the Si substrate just the CTE of the perovskite is effective, α_{per} . However, expansion of the layer is prohibited due to the high-modulus substrate and due to the pressure applied by the stamp; the stamp sets a hard ‘boundary’ and prevents bending. Hence, the strain is

negligible; instead a biaxial stress develops, corresponding to the respective temperature difference, ΔT (according to $\sigma_{th} = E^* \cdot \alpha_{per} \Delta T$). With 150 °C, our imprint temperature, a worst-case scenario would feature $\Delta T_{max} = 125K$; then, the layer was stress-free at room temperature (≈ 25 °C) before imprint. Conversely, a best-case scenario indicates a $\Delta T_{min} = 25K$, namely when the layer soft baked at 125 °C has not relaxed any residual stress due to cooling before imprint. With a linear CTE of $\alpha_{per} = 6.3 \cdot 10^{-5}/K$ obtained for a single crystal [61], this leads to thermal stresses in the range $85MPa \leq \sigma_{th} \leq 420MPa$. With polycrystalline layers, the CTE may even be higher than with a single crystal [62], resulting in somewhat higher thermal stress. (With N₂-anneal, the stress situation is almost comparable; sample bending may reduce the stress slightly, but due to the high modulus of the Si substrate stress relaxation is even so largely prohibited.) As the imprint pressure applied prevents bending it maximizes the thermal stress in the layer.

In total, the stresses resulting from all these sources sum up to $\sigma = \sigma_{th} + \sigma_p - \sigma_{gr}$. Initially, with $\sigma_{gr} \approx 0$, we have $\sigma = \sigma_{th} + \sigma_p \approx (85 - 420)MPa$, in a late growth state with $\sigma_{gr,max}$ we are in the range of $\sigma = (35 - 370)MPa$. The total stress is dominated by the thermal component; the fact that σ_p is negligible may be the reason why the application of pressure only did not result in grain growth (see Sect. 3.2.2).

Irrespective of the particular origin the stress existing in a layer represents a driving force for grain growth, more precisely for secondary, orientation-dependent coarsening. The driving force can be estimated [27, 63] according to $F_\sigma = (\sigma^2/2) \cdot (1/E_1^* - 1/E_2^*)$; the values E_1^* and E_2^* refer to adjacent grains with a differing orientation in vertical direction, e.g. grains with a (111) and a (100)-texture. Based on the literature values [58] ($E_1^* = E_{111}^* \approx 33GPa$, $E_2^* = E_{100}^* \approx 54GPa$), this results in a range of driving forces of about $10kPa \leq F_\sigma \leq 1MPa$.

To assess these values, a comparison with the capillary driving force based on grain curvature is helpful. It decreases with ongoing grain growth ($F_{cap} = \gamma_{gb}/\bar{r}$); an estimation based on $\gamma_{gb} \approx \gamma_{s0}/2 \approx 40mN/m$ and $\bar{r} \approx D_m/2$ results in values of $F_{cap} \approx 1.6MPa (D_m = 50nm)$ and $F_{cap} \approx 80kPa (D_m = 1\mu m)$. Thus, at high thermal stress a situation with $F_\sigma \approx F_{cap}$ may be reached during growth at a specific grain size; Fig. S-14 in the Supporting Information shows this graphically. Then, stress is a significant driver, whereas a low thermal stress is negligible in this respect.

Similar to surface energy, stress contributes to secondary, orientation-dependent growth [17]; it would favour the growth of grains with a low elastic energy at the cost of those with a higher elastic energy. At a state of stress with negligible strain (as it is the case with imprint), the elastic energy per volume amounts to $w_{el} = \sigma^2/2E^*$; hence, stress would favour the growth of grains featuring the highest biaxial modulus, in case of MAPbBr₃ grains with a

(100)-texture. In fact, our layers already feature a dominating (100)-orientation before imprint (compare Sect. 3.1.1); this means that in case that stress is relevant as a driving force (high thermal stress), it will improve the existing grain orientation by eliminating grains with a texture differing from the preferred (100). This is similar to the role of surface energy which would favour the growth of grains featuring the lowest surface energy possible with perovskites, grains with a (100)-texture with MAPbBr₃. Different from typical situations with annealing of metal layers [17, 28], both secondary driving forces favour a similar orientation with our perovskite, (100). Hence, thermal imprint offers optimal conditions to achieve a pronounced (100)-texture with MAPbBr₃ films, independent from the layer thickness.

To summarize, stress-related driving forces and capillary driving forces may feature a similar order of magnitude with thermal imprint. However, with pre-oriented MAPbBr₃ layers the role of stress (and surface energy) is to improve grain orientation, whereas grain growth primarily results from capillary forces.

3.2.6 Activation energy

Now, as grain growth with MAPbBr₃ in our imprint situation is well described by the general growth law, Eq. (2), with an exponent of $n \approx 3.4$, the physics may be investigated further, namely the specific temperature behaviour applying. This requires knowledge of the activation energy Q_n which is the reference to rate the thermal energy provided with respect to grain boundary mobility and thus grain growth (Arrhenius behaviour). With our basic discussion (Fig. 3), a value from literature was taken, $Q_n = 0.76\text{eV}$, determined by assuming ‘normal’ growth with $n = 2$ [12]; the perovskite in this reference was different from MAPbBr₃.

To find the activation energy relevant to our material, growth experiments were performed at 125 °C, 150 °C and 180 °C and the respective mean grain sizes D_m were evaluated. Plotting $\log(D_m^n - D_0^n)$ with $n = 3.4$ as a function of $1/T$ provides a straight line (see Supporting Information, Fig. S-15); its slope results in an activation energy of $Q_n = 1.19\text{eV}$. To compare with the literature, a growth law-independent activation energy is appropriate ($Q = Q_n/n$); Q_n is not a pure material constant but is correlated with the growth exponent according to Eq. (2). We find that our result $Q = 1.19\text{eV}/3.4 = 0.35\text{eV}$ is well in accord with activation energies obtained for hybrid perovskites by other groups ($Q = 0.76\text{eV}/2 = 0.38\text{eV}$ [12] and $Q = 0.3\text{eV}$ [56]). With specific values for the activation energy Q_n and the growth exponent n at hand, grain growth may now be re-plotted for our specific case, according to Eq. (2).

Figure 8 gives this theoretical relationship with our parameters. These diagrams are well suited for reasoning the consequences of choosing a specific processing temperature

and processing time with respect to grain growth with our material. The general consequences are similar as with Fig. 2; however, Fig. 8 allows to quantify them for our material system and our processing.

In particular, Fig. 8b may explain our experiment at 80 °C. In order to induce grain growth at this temperature, the 60-min imprint was too short; efficient grain growth within 60 min would require temperatures of at least 120 °C with our material. However, at long sight growth will occur at 80 °C as well and may change the properties of devices prepared from the perovskite, as e.g. an issue with solar cells under operation. Then, a precautionary measure is to have large grains in the device just after preparation; the larger these initial grains, the higher the temperature and the longer the time allowed without further grain growth, holding the risk of a potential change of the device properties low (– growth roughly starts when the exponential term for the temperature in question equals the already existing grain size, see Supporting Information Fig. S-5). With our

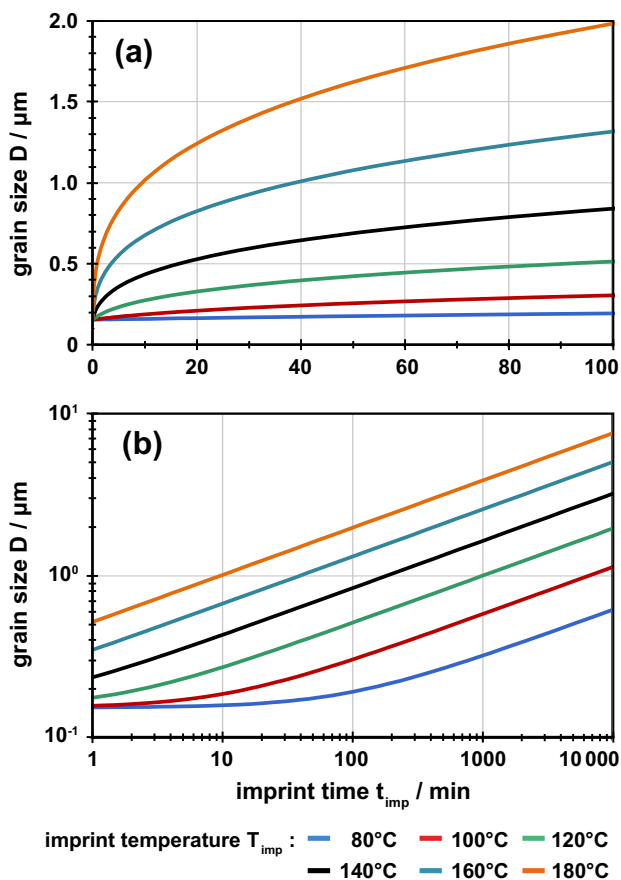


Fig. 8 Re-plot of the theoretical relationship with the parameters specific of our material and processing, namely $n = 3.43$, $Q_n = 1.19\text{eV}$ and an initial grain size $D_0 = 150\text{nm}$; a) linear plot, b) double-log plot over larger range. The temperatures are similar to Fig. 2, from 80 °C to 180 °C, in steps of 20 °C. The dominating initial grain size is most distinct with the double-log plot

material, a mean grain size of about 600 nm after device preparation would postpone a growth-induced change at 80 °C to times > 10⁴min (≈ 170h).

Moreover, it is now possible to check how well grain growth with our material is described by the growth law, Eq. (2). Figure 9 compares our data, those obtained with the PHP experiment and with HL (‘imprinted’ part) with the growth law, indicated as a continuous line with our conditions ($T = 150^{\circ}\text{C}$, $n = 3.43$, $Q_n = 1.19\text{eV}$). (A logarithmic view accentuates details of the initial phase, see Supporting Information Fig. S-17.) Including the PHP result (a grain size of about 570 nm after heat-up and a grain size of about 610 nm after an additional imprint of 5 min at 150 °C) in Fig. 9 required to define an ‘equivalent’ time t_{equ} that represents grain growth during the non-isothermal heat-up phase to 150 °C. The data points fit well with the simulation for the HL experiments when $t_{equ} = 11\text{min}$. This value is coherent with the specific heat-up characteristics of our system (see Fig. S-2, Supporting Information). It is slightly longer than the time span where the temperature is in the range of 140–150 °C. Obviously, the time span with temperatures below ≈140 °C is of minor impact with respect to grain growth; of course, this estimation refers to our equipment and will vary from system to system.

Figure 9 documents that our data are well represented by the simulation, in particular with imprint times of 5 min and beyond (stationary growth regime).

3.2.7 Impact of material choice

To address the choice of the material, a HL experiment similar to Fig. 7 was performed, however, with a layer prepared from a different Pb-precursor; instead of the Pb(Ac)₂ used with the experiments so far (from here on called material

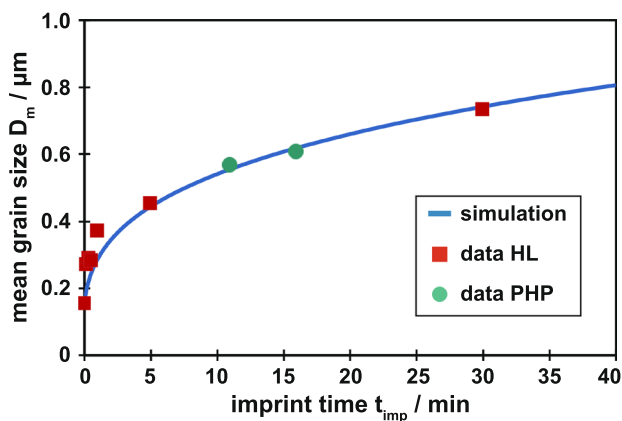


Fig. 9 Comparison of experimental data obtained with HL and with PHP with the growth law, based on our specific parameters ($T = 150^{\circ}\text{C}$, $n = 3.43$, $Q_n = 1.19\text{eV}$). (Estimated equivalent time for growth during heat-up with PHP: $t_{equ} = 11\text{min}$)

A), an acetate trihydrate was used, Pb(Ac)₂·3H₂O (material B). Though not the first choice due to the water content, this material offers a superior purity, 99.999%; the lead acetate of material A is specified with 99.8% by the supplier. As the soft bake was performed at 125 °C, we presume that the pristine layers prepared from material B are water-free [21].

The result for development of the grain size is presented in Fig. 10a. We focus on the main issue, grain growth (additional information is given in the Supporting Information, Fig. S-16). The growth law, Eq. (2), is still adequate for the whole regime investigated. Again, the slope in the ‘annealed’ part (0.18) is lower than in the ‘imprinted’ part (0.33).

Interestingly, both slopes are somewhat higher than with material A (Fig. 7c). Comparing the ‘imprinted’ parts, material B follows a growth law with a slightly smaller exponent, $n \approx 3.1$, whereas material A featured $n \approx 3.4$. Accordingly, grain growth proceeds somewhat faster with the higher purity material. In addition, comparing the absolute values with both materials, the grain sizes are about a factor of 4 higher with material B, see Fig. 10b; this is an even more dramatic difference than the differing exponent. Reconsidering the theoretical basis, at similar temperature a factor of 4 in grain size would require a 64-times longer anneal with $n = 3$ or, alternatively, an increase in the temperature by about 60 °C at constant time (as estimated from Fig. 8b). In view of a realistic procedure with a limited time and temperature allowed, these results suggest that purity of the materials is vital to obtain large grains. In view of the growth law, the results suggest that purity affects two parameters, the grain boundary mobility M and, to a lesser extent, also the growth exponent n .

The role of impurities during grain growth has also been addressed in the literature, with metals and semiconductors as well, where dissolved (atomic) impurities and larger particles or precipitates are discriminated [16]. With our material, both types may be present; atomic impurities may represent a part of the total amount of 0.2% in material A being not further specified; precipitates may refer to (ionic) compounds like Pb(OH)₂ and PbBr₂ (from degradation) or e.g. precursor residues (non-stoichiometric layer composition) [21].

During growth, dissolved impurities and small particles move together with the grain boundaries but reduce their velocity and thus the growth rate [46, 64]. Being expelled from the growing grains, impurities will accumulate at the grain boundaries. Resulting larger particles or precipitates are rather immobile; during grain growth the grain boundaries have to move round them [64]. The precipitates exert a drag force on the grain boundaries, the ‘Zener’ drag force F_Z [65] that counteracts growth. To compare it with the capillary driving force F_{cap} for grain growth ($F_{cap} = \gamma_{gb}/\bar{r}$), the Zener drag force can be expressed by means of an effective radius of the precipitates, R_{eff} , according to $F_Z \propto \gamma_{gb}/R_{eff}$, with $R_{eff} \approx r_p/f_p$

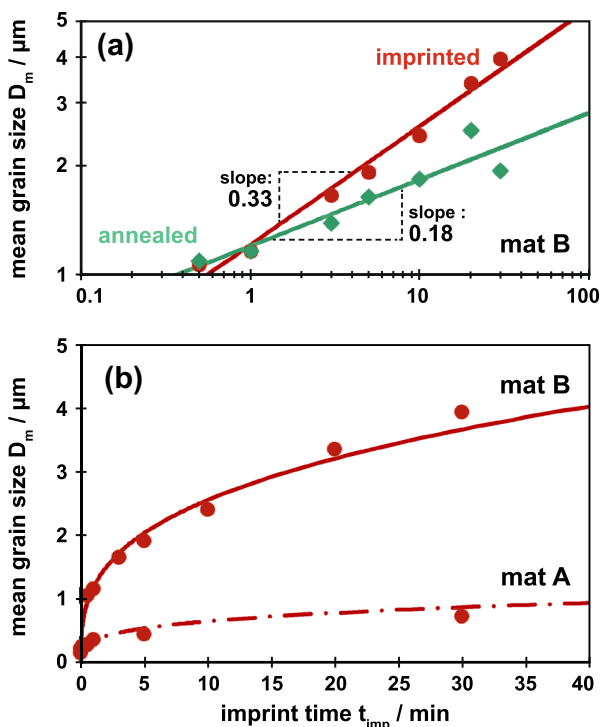


Fig. 10 HL experiments at 150 °C (soft bake 125 °C, 2 min). **a** Increase in the mean grain size for the ‘imprinted’ part and the ‘annealed’ part of the sample prepared with material B (precursor solution with high-purity lead acetate trihydrate); overall slopes 0.33 ($n_{est} = 3.1$) and 0.18 ($n_{est} = 5.6$). Evaluation from $D_m > 2D_0$ results in similar values ($n_{est} \equiv n$), as all evaluated grain sizes are well beyond this boundary ($D_0 = 230nm$). All data refer to samples from the same batch. **b** Comparison of mean grain size in the ‘imprinted’ parts with samples prepared from material A (dash–dotted line) and the high-purity material B (full line)

(r_p the particle radius and f_p its respective volume amount) [64]. With $F_Z = F_{cap}$, an equilibrium is reached where grain growth stops. According to this physical perception, stagnation induced by precipitates is accounted for. The grain boundaries become ‘pinned’ locally, with $D_{pin} \propto r_p / (f_p)^{1/2}$. As our experiments did not indicate any stagnation even with the material of limited purity (compare long-time experiment in Fig. 7c), large precipitates seem not to be an issue with our preparation.

However, the effect of impurities and/or small particles in reducing grain growth is clearly indicated by the experiments. Beyond the slightly different growth exponent n , we expect that the main effect of purity is on the activation energy Q and on the pre-factor M_0 . With a high purity of the polycrystalline

layer, the energy required to move the grain boundaries is low when the respective barrier, Q , is low [27].

With respect to grain growth, we conclude that the choice of materials of highest possible purity is essential (with all components of the precursor solution) when large grains are envisaged. However, just as important is the preparation of highly stoichiometric layers to minimize non-perovskite impurities/particles or precipitates in the layer. Beyond a diligent weight ratio, a complete solution in the solvent is indispensable avoiding any filtration.

3.3 Consequences

The investigation presented allows to draw consequences with respect to the physical basics underlying grain growth and, moreover, with respect to proceeding in praxis.

The results demonstrate that the concepts for grain growth developed with metals and classical semiconductors are well applicable to polycrystalline perovskite layers. However, due to their surface-induced nucleation during layer formation the grains feature a distinct orientation from the beginning. As a consequence, the conventional classification into ‘normal’ and ‘secondary’ growth in its original meaning does not apply. In return, the exponential characteristics of the growth law are clearly displayed by the experiments.

The specific interface energies prevailing at the substrate and at the stamp are not in conflict with grain growth. On the contrary, they support the formation of large grains spanning the whole layer thickness; the flat surface is beneficial to the preparation of multi-layer devices.

The primary parameter for grain growth during imprint is the processing temperature; it provides the mobility of the grain boundaries required. In addition to the capillarity-induced driving force, also thermal stresses may be operative; if present, the latter will support the development of a (100)-orientation of MAPbBr₃ grains. This is similar with N₂-anneal and may be the reason why stationary growth during thermal treatment is largely independent from the process chosen, imprint or anneal in nitrogen. With pre-oriented grains, stress will improve the orientation. The role of the external imprint pressure with grain growth is to maximize the thermal stress by preventing sample bending. In addition, it may postpone any stagnation of growth by suppressing grooving.

The capillarity-based growth law describes grain growth in our polycrystalline MAPbBr₃ perovskite layers well, with an activation energy of $Q \approx 0.35eV$ and a growth exponent of $n \approx 3.4$. With stoichiometric layers prepared from highest purity materials, larger grains are obtained under otherwise similar conditions, most likely due to a facilitated

grain boundary movement resulting, for example, from a decreased activation energy.

Our impression is that the physical basis worked out here with MAPbBr₃ is applicable to other polycrystalline materials, in particular other perovskites. It is in particular suited to define a procedure to characterize grain growth in a polycrystalline layer with a limited number of experiments.

In praxis, we suggest that the parameters obtained with our material ($n \approx 3$, $Q_n \approx 1\text{eV}$) are a good starting point to reflect on the effect of temperature during grain growth. With an unknown perovskite material (at a specific, invariant preparation of the layers), a determination of the respective parameters, n and Q (or rather n_{est} and Q_n in the first instance), is required.

In a first step, n_{est} is determined. For this purpose, imprint experiments (or annealing experiments) for highly differing times (well distributed on a logarithmic scale) have to be performed and the respective mean grain size has to be evaluated; we propose to average over about 500 grains. As in general, an imprint system will not provide experiments with $T = const$ from loading on (as with our HL experiments); a conventional imprint system has to be used, particularly a PHP process; this system will feature its own heat-up characteristics. However, this heat-up phase can be accounted for quite easily. As the growth law, Eq. (2), starts from a certain ‘initial grain size’ anyway—with our experiments, it was the grain size of the pristine layer—we may take the grain size after heat-up as the ‘initial grain size’ for evaluation, $D_0 \equiv D_{heat-up}$. Then, for evaluation the time is the actual imprint time (starting after heat-up only); just the isothermal ‘imprint’ time is evaluated (see Fig. 1a). As grains may not differ too much from this D_0 with small imprint times (as with our PHP experiment, paragraph 3.1.3), the exponent n_{est} (evaluated from a double-log plot of the results, similar to Fig. 7c or Fig. 10a) may be an upper limit only.

In a second step, the activation energy Q_n has to be determined. The mean grain sizes of experiments at e.g. three different temperatures (similar to Fig. S-15) provide Q_n from the slope over $1/T$ when $D_m^n - D_0^n$ is plotted ($-D_0$ may vary with the imprint temperature chosen). Assuming $n \approx n_{est}$ provides $Q = Q_n/n_{est}$.

In a third step, some refinement is feasible (if reasonable) by simulating grain growth with this parameter set, n_{est} and Q , and refining towards somewhat lower n -values. A double-log representation is beneficial to rate the quality of the simulation to reproduce the experimental values; an example is given in the Supporting Information, Fig. S-18.

With the parameters n and Q_n (or Q) on hand, the potential of the material in question with respect to grain growth (or its prevention) can be assessed. However, it should be kept in mind that any change of the preparation or e.g. ageing of the precursor solution may alter the results obtained.

Diligence of preparation is as important as the use of high-purity materials.

4 Summary and conclusions

The investigation has shown that the main parameter responsible for grain growth with MAPbBr₃ during thermal imprint is the temperature, where the pressure applied to the stamp maximizes thermal stress and may prevent grooving-induced stagnation. Though a classification into ‘normal’ and ‘secondary’ growth does not apply, the growth behaviour is well described by a capillary-based growth law, with $D_m^n - D_0^n \propto \exp(-Q_n/kT) \cdot t$. We evaluated the growth exponent n from isothermal ‘hot loading’ experiments for times of 10 s to 1 day; the activation energy Q_n was determined from experiments in the temperature range of 120–180 °C. Characteristic values are $n \approx 3$ and $Q_n \approx 1\text{eV}$ ($Q \approx 0.3\text{eV}$). Our experiments are well described by theory so that simulation allows to rate and to predict the growth behaviour with differing times and/or temperatures. Material purity turned out to be decisive to obtain large grains; however, a diligent and always similar preparation is equally important.

Beyond grain growth the results and consequences are valuable to assess the stability of polycrystalline perovskite layers (no further grain growth) under specific operating conditions.

Supplementary Information The online version contains supplementary material available at <https://doi.org/10.1007/s00339-021-04830-0>.

Funding Open Access funding enabled and organized by Projekt DEAL. Financial support from the Deutsche Forschungsgemeinschaft (DFG) is highly acknowledged (contracts RI 1551/9-1 and SCHE 580/23-1).

Open Access This article is licensed under a Creative Commons Attribution 4.0 International License, which permits use, sharing, adaptation, distribution and reproduction in any medium or format, as long as you give appropriate credit to the original author(s) and the source, provide a link to the Creative Commons licence, and indicate if changes were made. The images or other third party material in this article are included in the article's Creative Commons licence, unless indicated otherwise in a credit line to the material. If material is not included in the article's Creative Commons licence and your intended use is not permitted by statutory regulation or exceeds the permitted use, you will need to obtain permission directly from the copyright holder. To view a copy of this licence, visit <http://creativecommons.org/licenses/by/4.0/>.

References:

1. C.V. Thompson, Annu. Rev. Mater. Sci. **30**, 159 (2000)
2. C. Pan, L. Zhang, W. Jiang, W. Setyawan, L. Chen, Z. Li, N. Liu, T. Wang, J. Eur. Ceram. Soc. **40**, 4396 (2020)

3. Y. Mutoh, Y. Miyashita, T. Hansson, M. Takahashi, in *Plastic Deformation of Ceramics*. ed. by R.C. Bradt, C.A. Brookes, J.L. Routbort (Springer, US, Boston, MA, 1995), pp. 653–666
4. P. Das, S. Bathula, and S. Gollapudi, *Nano Express* **1**, 020036 (2020).
5. H. Dong, B. Wen, R. Melnik, *Sci. Rep.* **4**, 7037 (2014)
6. B.P. Tyagi, K. Sen, *Phys. Status Solidi A* **85**, 603 (1984)
7. L. Cao, K. J. Ganesh, L. Zhang, O. Aubel, C. Hennesthal, M. Hauschildt, P. J. Ferreira, and P. S. Ho, *Appl. Phys. Lett.* **102**, 131907 (2013).
8. A.V. Krishnamoorthy, P.J. Marchand, F.E. Kiamilev, S.C. Esener, *Appl. Opt.* **31**, 5480 (1992)
9. S. Kumari, N.K. Arora, G.C. Jain, *Sol. Energy Mater.* **5**, 383 (1981)
10. S.-Y. Kim, J.K. Park, W.S. Hwang, S.-J. Lee, K.-H. Lee, S.H. Pyi, B.J. Cho, *J. Nanosci. Nanotechnol.* **16**, 5044 (2016)
11. J. Chen, J. Suwardy, T. Subramani, W. Jevasuwan, T. Takei, K. Toko, T. Suemasu, N. Fukata, *CrystEngComm* **19**, 2305 (2017)
12. C. Ji, C. Liang, H. Zhang, M. Sun, Q. Song, F. Sun, X. Feng, N. Liu, H. Gong, D. Li, F. You, Z. He, A.C.S. *Appl. Mater. Interfaces* **12**, 20026 (2020)
13. J. Moon, S. Kwon, M. Alahbakhshi, Y. Lee, K. Cho, A. Zakhidov, M.J. Kim, Q. Gu, A.C.S. *Appl. Mater. Interfaces* **13**, 5368 (2021)
14. C. Liu, Y.-B. Cheng, Z. Ge, *Chem. Soc. Rev.* **49**, 1653 (2020)
15. A. Dualeh, N. Tétreault, T. Moehl, P. Gao, M.K. Nazeeruddin, M. Grätzel, *Adv. Funct. Mater.* **24**, 3250 (2014)
16. C.V. Thompson, *Annu. Rev. Mater. Sci.* **20**, 245 (1990)
17. C.V. Thompson, R. Carel, *Mater. Sci. and Eng. B-Adv.* **32**, 211 (1995)
18. T. Seewald, E. R. Schütz, C. Ebenhoch, and L. Schmidt-Mende, *J. Phys. Energy* **2**, 021001 (2020).
19. C.V. Thompson, *Mater. Sci. Forum* **94–96**, 245 (1992)
20. A. Mayer, M. Buchmüller, S. Wang, C. Steinberg, M. Papenheim, H.-C. Scheer, N. Pourdavoud, T. Haeger, T. Riedl, *J. Vac. Sci. Technol. B* **35**, 06G803 (2017)
21. A. Mayer, N. Pourdavoud, Z. Doukkali, K. Brinkmann, J. Rond, J. Staabs, A.-C. Swertz, F. van gen Hassend, P. Görrn, T. Riedl, and H.-C. Scheer, *Appl. Phys. A* **127**, 237 (2021).
22. N. Pourdavoud, S. Wang, A. Mayer, T. Hu, Y. Chen, A. Marjanovich, W. Kowalsky, R. Heiderhoff, H.-C. Scheer, T. Riedl, *Adv. Mater.* **29**, 1605003 (2017)
23. N. Pourdavoud, A. Mayer, M. Buchmüller, K. Brinkmann, T. Häger, T. Hu, R. Heiderhoff, I. Shutsko, P. Görrn, Y. Chen, H.-C. Scheer, T. Riedl, *Adv. Mater. Technol.* **3**, 1700253 (2018)
24. N. Pourdavoud, T. Haeger, A. Mayer, P.J. Cegielski, A.L. Giesecke, R. Heiderhoff, S. Olthof, S. Zaefferer, I. Shutsko, A. Henkel, D. Becker-Koch, M. Stein, M. Cehovski, O. Charfi, H. Johannes, D. Rogalla, M.C. Lemme, M. Koch, Y. Vaynzof, K. Meerholz, W. Kowalsky, H. Scheer, P. Görrn, T. Riedl, *Adv. Mater.* **31**, 1903717 (2019)
25. C.V. Thompson, *MRS Proc.* **280**, 307 (1992)
26. C.V. Thompson, H.I. Smith, *Appl. Phys. Lett.* **44**, 603 (1984)
27. C.V. Thompson, *J. Appl. Phys.* **58**, 763 (1985)
28. C.V. Thompson, *Interface Sci.* **6**, 85 (1998)
29. R. Carel, *Grain Growth and Texture Evolution in Thin Films*, PhD Thesis, Massachusetts Institute of Technology, 1995.
30. W.W. Mullins, *Acta Metall.* **6**, 414 (1958)
31. W.W. Mullins, *J. Appl. Phys.* **28**, 333 (1957)
32. C.S. Smith, *Metall. Rev.* **9**, 1 (1964)
33. H. Wang, R. Haroldson, B. Balachandran, A. Zakhidov, S. Sohal, J.Y. Chan, A. Zakhidov, W. Hu, *ACS Nano* **10**, 10921 (2016)
34. C. Steinberg, K. Dhima, D. Blenskens, A. Mayer, S. Wang, M. Papenheim, H.-C. Scheer, J. Zajadacz, K. Zimmer, *Microelectron. Eng.* **123**, 4 (2014)
35. A. Mayer, S. Moellenbeck, K. Dhima, S. Wang, and H.-C. Scheer, *J. Vac. Sci. Technol. B* **29**, 06FC13 (2011).
36. A. Mayer, K. Dhima, S. Möllenbeck, S. Wang, H.-C. Scheer, *Proc. SPIE* **8352**, 83520N (2012)
37. C. Bi, Q. Wang, Y. Shao, Y. Yuan, Z. Xiao, J. Huang, *Nat. Commun.* **6**, 7747 (2015)
38. J. Ding, Y. Zhao, S. Du, Y. Sun, H. Cui, X. Zhan, X. Cheng, L. Jing, *J. Mater. Sci.* **52**, 7907 (2017)
39. P.A. Beck, *JOM* **2**, 468 (1950)
40. P.A. Beck, P.R. Sperry, *J. Appl. Phys.* **21**, 150 (1950)
41. J.E. Palmer, C.V. Thompson, H.I. Smith, *J. Appl. Phys.* **62**, 2492 (1987)
42. R. Venkatraman, J.C. Bravman, *J. Mater. Res.* **7**, 2040 (1992)
43. T. Wang, G. Lian, L. Huang, F. Zhu, D. Cui, Q. Wang, Q. Meng, C.-P. Wong, A.C.S. *Appl. Mater. Interfaces* **12**, 38314 (2020)
44. J. Xiao, Y. Yang, X. Xu, J. Shi, L. Zhu, S. Lv, H. Wu, Y. Luo, D. Li, Q. Meng, *J. Mater. Chem. A* **3**, 5289 (2015)
45. A. Rollett, *Scr. Mater.* **36**, 975 (1997)
46. C. Weyrich, *Z. Naturforsch.* **26**, 1198 (1971)
47. R. Schmager, I. M. Hossain, F. Schackmar, B. S. Richards, G. Gomard, and U. W. Paetzold, *Sol. Energy Mater. Sol. Cells* **201**, 110080 (2019).
48. S. V. Makarov, V. Milichko, E. V. Ushakova, M. Omelyanovich, A. Cerdan Pasaran, R. Haroldson, B. Balachandran, H. Wang, W. Hu, Y. S. Kivshar, and A. A. Zakhidov, *ACS Photonics* **4**, 728 (2017).
49. Z. Xiao, Q. Dong, C. Bi, Y. Shao, Y. Yuan, J. Huang, *Adv. Mater.* **26**, 6503 (2014)
50. P.R. Rios, D. Zöllner, *Mater. Sci. Technol.* **34**, 629 (2018)
51. Y. Wang, X. Lü, W. Yang, T. Wen, L. Yang, X. Ren, L. Wang, Z. Lin, Y. Zhao, *J. Am. Chem. Soc.* **137**, 11144 (2015)
52. T. Matsushima, T. Fujihara, C. Qin, S. Terakawa, Y. Esaki, S. Hwang, A.S.D. Sandanayaka, W.J. Potscavage, C. Adachi, *J. Mater. Chem. A* **3**, 17780 (2015)
53. Y. Rakita, S.R. Cohen, N.K. Kedem, G. Hodes, D. Cahen, *MRS Commun.* **5**, 623 (2015)
54. R. Zhang, W. Cai, T. Bi, N. Zarifi, T. Terpstra, C. Zhang, Z.V. Verdeny, E. Zurek, S. Deemyad, *J. Phys. Chem. Lett.* **8**, 3457 (2017)
55. K.T. Miller, F.F. Lange, D.B. Marshall, *J. Mater. Res.* **5**, 10 (1990)
56. M. Jaysankar, W. Qiu, J. Bastos, J.G. Tait, M. Debucquoy, U.W. Paetzold, D. Cheyins, J. Poortmans, *J. Mater. Chem. A* **4**, 10524 (2016)
57. X. Cao, L. Zhi, Y. Li, F. Fang, X. Cui, L. Ci, K. Ding, J. Wei, A.C.S. *Appl. Energy Mater.* **1**, 868 (2018)
58. J. Feng, *APL Mater.* **2**, 081801 (2014).
59. W.D. Nix, *Metall. Mater. Trans. A* **20**, 2217 (1989)
60. A. B. Mei, R. B. Wilson, D. Li, D. G. Cahill, A. Rockett, J. Birch, L. Hultman, J. E. Greene, and I. Petrov, *J. Appl. Phys.* **115**, 214908 (2014).
61. M. Keshavarz, M. Ottesen, S. Wiedmann, M. Wharmby, R. Küchler, H. Yuan, E. Debroye, J.A. Steele, J. Martens, N.E. Hussey, M. Bremholm, M.B.J. Roefsaers, J. Hofkens, *Adv. Mater.* **31**, 1900521 (2019)
62. T. Haeger, R. Heiderhoff, T. Riedl, *J. Mater. Chem. C* **8**, 14289 (2020)
63. G. Gottstein, *Physikalische Grundlagen Der Materialkunde*, 3rd edn. (Springer, Berlin Heidelberg New York, 2007)
64. G.S. Rohrer, *Metall. and Mat. Trans. A* **41**, 1063 (2010)
65. E. Nes, N. Ryum, O. Hunderi, *Acta Metall.* **33**, 11 (1985)

Publisher's Note Springer Nature remains neutral with regard to jurisdictional claims in published maps and institutional affiliations.